

Received September 13, 2019, accepted November 6, 2019, date of publication November 11, 2019, date of current version November 21, 2019.

Digital Object Identifier 10.1109/ACCESS.2019.2952893

Electromagnetic Design and Analysis of Axial Flux Permanent Magnet Generator With Unequal-Width PCB Winding

XIAOYUAN WANG¹, WEI PANG¹, PENG GAO^{1,2}, AND XIAOXIAO ZHAO¹

¹School of Electrical and Information Engineering, Tianjin University, Tianjin 300072, China

²Xi'an Micromotor Research Institute, Xi'an 710077, China

Corresponding author: Peng Gao (gaopeng218@tju.edu.cn)

This work was supported by the National Natural Science Foundation of China under Grant 51577125.

ABSTRACT For the design of printed circuit board (PCB) winding, it is necessary to take into account the requirements of electromagnetic and manufacture technology of PCB winding, which directly affect the output power of the machine. In this paper, for axial flux permanent magnet generator (AFPMG) of a small wind power system, the unequal-width (UEW) winding is proposed for the aim of improving the output power of the generator. The design ideas and methods of unequal-width (UEW) winding are proposed in combination with manufacture technology of the PCB. The finite element analysis (FEA) model of machine is built. The analytical formulas of electromotive force (EMF) and winding loss are derived. Though the comparisons between reactance and impedance of PCB winding, the analytical formula of output power is simplified. These characteristics of the generator with traditional equal-width (EW) winding and proposed UEW winding are analyzed and compared in detail by FEA and analytical calculation. The result shows that the output power of the generator with UEW winding is improved largely. Finally, the validity of the FEA model and analysis method is verified by experiment of prototype machine, which provides the reference for the design of AFPMG with PCB winding.


INDEX TERMS Axial flux motor, analytical calculation, finite element analysis (FEA), generator, ironless stator, output power, printed circuit board (PCB) winding, winding design.

I. INTRODUCTION

This Axial flux permanent magnet (AFPM) machine, known as a disc permanent magnet machine, has the characteristics of short axial dimension, high efficiency and high power density [1]–[4]. As a new generation of high-performance servo and high-torque direct drive motors, it is especially suitable for electric vehicles, wind turbines for wind generation [5]–[8] and aerospace actuators [9]. For AFPM machine with printed circuit board (PCB) winding, its stator iron is removed, which reduces the weight of the machine and eliminates iron loss and cogging torque [10]. At present, it is relatively a mature technology that makes the design of PCB winding more flexible and the position of winding more accurate in the production technology [11]. It benefits the accurate calculation for the inductance, back electromotive

force (EMF) and relevant parameters of the machine. The small thickness of PCB winding can also reduce the air gap length of machine [12], which makes the axial space of machine more compact.

It's crucial for the design towards PCB winding to improve the output power of axial flux permanent magnet generator (AFPMG). In [13], the PCB wedge shape winding for low-speed ocean current generator is designed, in order to eliminate cogging torque, avoid any slip rings, and remove the gearbox between turbine and generator which increases the weight and noise of turbine. However, the size design methods for the equal-width wedge shape winding has not been proposed. Thus, it's difficult to further optimize the wedge shape winding in detail to increase the output power of the generator. The non-overlapping concentrated PCB stator applied to AFPMG for small-scale off-grid wind turbine has been proposed in [14]. It gives three recommendations that may improve the output power of generator, such as reducing

The associate editor coordinating the review of this manuscript and approving it for publication was Alfeu J. Sguarezi Filho .

air gap from magnet to stator, using lower resistance bearing and obtaining more complete power curve to find peak power point. But there is no recommendation for optimizing some dimensions of the PCB stator to improve the output power of generator. In [15], a novel rhomboidal PCB winding applied to a miniature axial-flux spindle motor has been designed to minimize the copper loss. The variations of turns and line width for rhomboidal winding can cause variations of winding resistance and eddy current losses in the winding. If combining with the production technology of PCB, the number of turns and line width of PCB winding may be synergistically optimized, which may further reduce the copper losses and improve the output power of the generator.

Aiming at improving the output power of AFPM generators applied to small wind power generation systems, this paper proposes a new type of unequal width (UEW) concentric spiral winding by combining with PCB production technology. The proposed UEW PCB winding is also designed to reduce winding resistance and increase the copper percentage on the PCB board, which is beneficial to the heat dissipation of the PCB board. Its design ideas and theoretical design formulas for the main parameters of PCB winding are proposed. In order to reduce the winding resistance and further improve the output power of the generator, a multi-layer parallel winding structure is adopted. Considering the impact of eddy current losses in PCB winding, the eddy current losses in the equal width (EW) PCB winding and the UEW PCB winding are compared and analyzed by finite element analysis (FEA) and analytical calculation. Furthermore, the output performances at load of AFPMG with the two windings are compared and analyzed in detail. Finally, the proposed UEW PCB winding and prototype machine have been designed and manufactured. The validity of the FEA and analytical calculation is verified by the prototype experiment, which provides theoretical and engineering application reference for the research of AFPMG and the proposed design of PCB winding.

II. BASIC PRINCIPLE OF AFPMG WITH PCB WINDING

The basic structure of AFPMG with PCB winding and double outer rotor is shown in Fig. 1.

A. THE KEY DESIGNS OF PCB WINDING WITH UEW

In this section, the PCB winding is designed using the concept of concentric spiral winding. The UEW winding is designed and proposed by widening active conductor of EW toward both sides symmetrically, in order to make full use of extra insulation space between the active conductors. Comparing with traditional EW PCB winding, the proposed UEW PCB winding has the advantages of smaller resistance, larger equivalent heat dissipation area (larger copper percentage on the PCB board) and average current carrying capacity. The proposed UEW active conductor and structure of concentric spiral PCB winding is shown in Fig. 2.

The design of PCB winding with the UEW active conductor and its inner and outer diameters is crucial for the design of

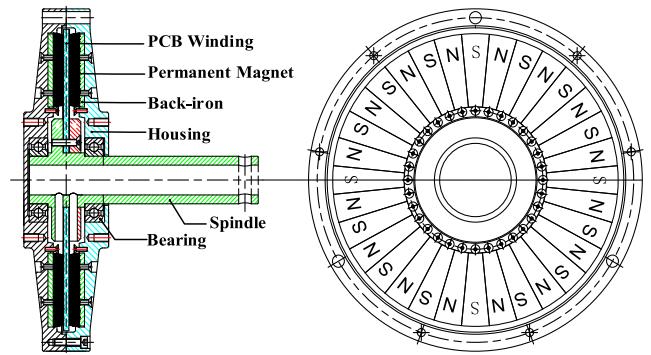


FIGURE 1. Structure diagram of AFPMG.

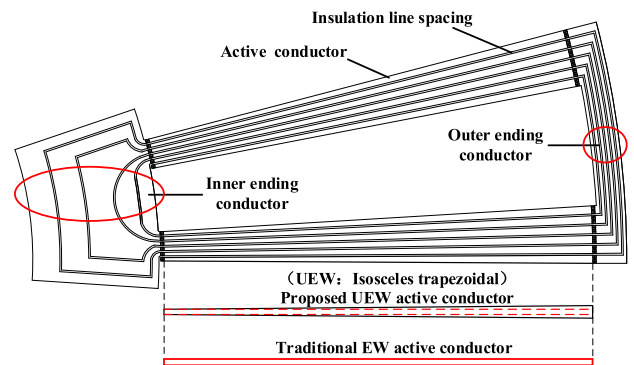


FIGURE 2. Structure diagram of concentric spiral PCB winding.

PCB winding. For the selection of inner and outer diameters of active conductor of PCB winding, some factors, such as outer-to-inner diameter ratio γ , the number of turns of active conductor, insulation gap and heat load at inner diameter, need to be considered. Generally, the outer-to-inner diameter ratio γ of AFPMG is between 1.5 and 2.2, and the ratio γ is 1.5 to 1.73 for small machine [16].

For the inner diameter design of active conductor of PCB winding, these required parameters in PCB process should be considered such as line width of conductor, insulation line space, number of turns per phase per pole, and heat load at inner diameter. The main design dimensions of PCB winding are shown in Fig. 3, where d_L is the insulation line space of active conductor. t_k is the thickness of each layer of copper foil. d_{oc} is the insulation space between connection conductors at the outer end. w_{oc} is the line width of connection conductor at the outer end. D_{mi} and D_{mo} are the diameters of inner end and outer end of active conductor respectively. w_{ie} and w_{oe} are the line widths at the inner end and outer end of the UEW active conductor respectively. The design of the inner diameter of PCB winding is usually considered together with the number of turns per phase per pole N whose expression is:

$$N = \frac{\pi D_{mi}}{2mp(w_{ie} + d_L)} \quad (1)$$

where N is the number of turns per phase per pole. m is the number of phases. p is the number of pole pair. It is shown

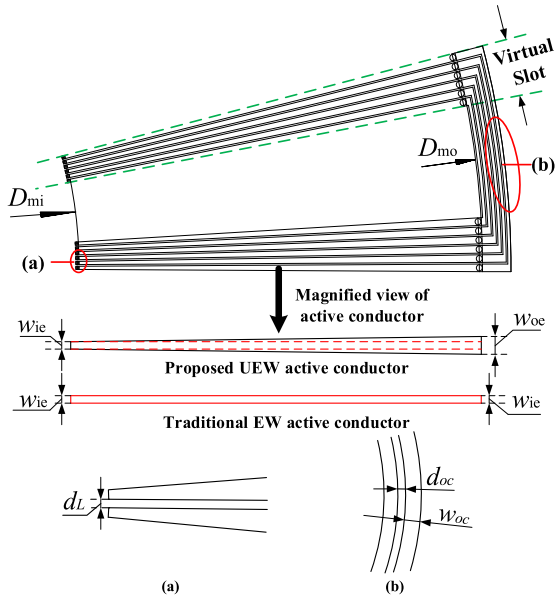


FIGURE 3. The main parametric design diagram of PCB winding. (a) Magnified view of active conductor at inner ending. (b) Magnified view of connection conductor at outer ending.

in (1) that in the case where w_{ie} and d_L are constant, the calculation value of N may not be an integer if D_{mi} is given first. Therefore, N is generally given first, then the design value of D_{mi} is calculated according to the given value of N .

It is important for the design of line width w_{ie} and insulation line spacing d_L in (1). For the design of line width w_{ie} , it needs to meet the requirement of through-hole processing size [17] since the inner end of active conductor needs to be connected with via holes. In case of meeting the above processing of PCB, the design value of line width w_{ie} can be obtained according to the current density at the inner end of active conductor. Because the current density at the inner end of the active conductor is largest and the heat generation is concentrated, thus the design of line width w_{ie} is reasonable according to it.

For the design of insulation line spacing d_L in [18], two conditions must be satisfied as follows: 1) the breakdown voltage of insulation spacing must be greater than the electrical potential difference between adjacent conductors. 2) As the thickness of copper foil each layer increases, the insulation gap needs to be increased accordingly. In this section, the insulation line spacing d_L of PCB winding is 0.3 mm and the thickness of copper foil each layer t_k is 4 oz (1 oz = 0.035 mm).

The outer diameter design of active conductor of PCB winding is related to the maximum size D_{max} of outer diameter of PCB winding, the number of turns per phase per pole N , the line width w_{oc} and insulation line spacing d_{oc} of connection conductor at outer end. In the right range of outer-to-inner diameter ratio γ , the expression of outer diameter D_{mo} of active conductor is:

$$D_{mo} = D_{max} - 2N(w_{oc} + d_{oc}) \quad (2)$$

TABLE 1. The parameters of the AFPMG.

Design data	value
Rated output power	240 W
Rated speed	300 r/min
Number of poles	32
Number of stator slots (virtual slot)	48
PCB outer diameter	222 mm
Air gap	0.9 mm
Thickness of permanent magnet (PM)	7.0 mm
Thickness of copper foil each layer	0.14 mm
Insulation spacing between conductors	0.3 mm
Thickness of PCB winding	3.2 mm
Number of PCB layers	12

For the design of line width w_{oe} at the outer end of the UEW active conductor, the design value of outer diameter D_{mo} of active conductor needs to be defined first. On this basis, the expression of w_{oe} can be derived as:

$$w_{oe} = \frac{\pi D_{mo}}{2mpN} - d_L \quad (3)$$

The number of the PCB winding layers are designed to be 12. They are divided into two parts (the upper 6 layers and the lower 6 layers), which are connected in serial to improve the output voltage of the machine. But the active conductors of the upper 6 layers or the lower 6 layers are connected in parallel to reduce the resistance and the copper losses of PCB winding. The AFPMG of PCB concentric distributed winding with 32 poles and 48 virtual slots is designed and shown in Fig. 3. The definition of virtual slot is that one coil side will be seen as a virtual slot. These main design parameters and design requirements of machine are shown in Table 1.

B. SIMULATION MODEL

In order to simplify calculation process and reduce time of simulation, the FEA model of three Dimension (3-D) of 1/16 machine is built and shown in Fig. 4. The FEA model of PCB winding is shown in Fig. 5.

III. MATHEMATICAL ANALYSES

A. BACK EMF

Copper conductor strips of PCB winding are distributed uniformly along the circumferential direction. When the machine is operating at no-load, an active conductor in one corner position θ is analysed in the plane of polar coordinate system (r, θ) . The average EMF E_c of active conductor is [16]:

$$E_c = \frac{1}{8} \Omega B_{\delta av} (D_{mo}^2 - D_{mi}^2) \quad (4)$$

where Ω is the mechanical angular velocity. $B_{\delta av}$ is the average of air gap flux density at a pole pitch, which is related to flux density amplitude B_m of air gap. The expression of B_m

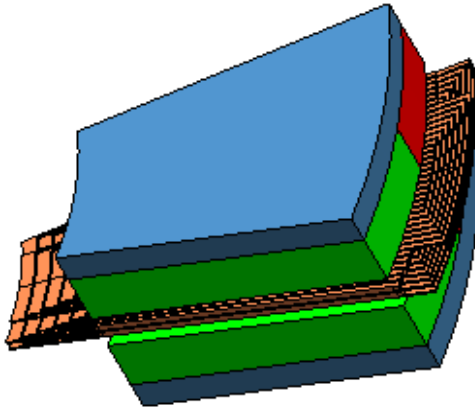


FIGURE 4. 3-D FE simulation model of 1/16 AFPMG with PCB winding.

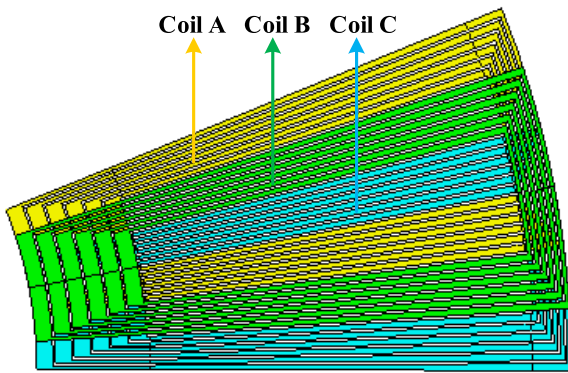


FIGURE 5. The equivalent model of PCB winding.

is:

$$B_{\delta_{av}} = \alpha_i B_m \quad (5)$$

where α_i is the calculation polar arc coefficient. Then the back-EMF E_ϕ of each phase can be deduced:

$$E_\phi = \sqrt{2}\pi f N_1 k_{w1} \Phi_m = \frac{\sqrt{2}\pi}{60} p n N_1 k_{w1} \Phi_m \quad (6)$$

where f is the frequency of back-EMF. k_{w1} is the winding coefficient. N_1 is the number of series turns of one branch in one phase. Φ_m is the magnetic flux amplitude per pole and its expression is:

$$\Phi_m = \alpha_i \frac{\pi}{p} B_m \int_{D_{mi/2}}^{D_{mo/2}} r dr = \frac{\pi}{8p} \alpha_i B_m (D_{mo}^2 - D_{mi}^2) \quad (7)$$

B. WINDING LOSS

When PCB generator is operating normally, the current of stator flowing into PCB winding will generate copper loss, which is the main heating source of machine. For the concentric spiral PCB winding, it can be assumed that the current is evenly distributed across conductors, the resistance r_0 of conductor can be expressed as:

$$r_0 = \rho \frac{\sum_{n=1}^{N_{max}} L_n}{S_L} \quad (8)$$

where ρ is the resistivity of copper conductor. L_n is the length of the n th turn. S_L is the average cross-sectional area of the conductor. Thus, the copper loss of winding can be obtained as follow:

$$p_{Cu} = I^2 r_0 = J^2 S_L \rho \sum_{n=1}^{N_{max}} L_n \quad (9)$$

where, I is the current of conductor. J is the average current density of conductor.

When alternating magnetic field changes with the time in axial air gap space, the eddy-current in PCB winding is induced to generate eddy-current loss of winding. The magnitude of eddy-current loss is related to the line width of conductor, the quality of conductor, the amplitude of flux density across conductor, and the alternating frequency of magnetic flux. The expression of eddy-current loss of PCB winding is [19]–[21]:

$$p_v = \frac{1}{\rho_L} \frac{\pi^2}{3\rho} f^2 w_L^2 m_c (B_{mt1}^2 + B_{ma1}^2) \eta_d^2 \quad (10)$$

where ρ is the resistivity of copper conductor. ρ_L is the density of copper conductor. f is the alternating frequency of magnetic field. w_L is the line width. m_c is the winding quality without connection conductors at inner and outer ends. B_{mt1} and B_{ma1} are the flux density peaks of fundamental wave in the directions of tangential and axial respectively. η_d is the waveform distortion coefficient of magnetic flux density.

C. REACTANCE AND IMPEDANCE

The inductance of PCB winding is relatively small because PCB winding is ironless. When the speed of machine is small, the impedance generated in PCB winding is mainly the winding resistance since winding reactance can be ignored. With the increases in speed of the generator, the reactance and impedance of the PCB winding are also increased, which can affect the output characteristic of generator. Therefore, it is important to calculate the inductance of winding in order to obtain the values of reactance and impedance of winding.

When the three-phase currents flow into PCB winding, the magnetic field of the armature is generated, which can cause the armature reaction in PCB generator. The fundamental amplitude of magnetomotive force F_1 is:

$$F_1 = \frac{m\sqrt{2}}{\pi} N_1 k_{w1} I_1 \quad (11)$$

where I_1 is the root mean square (rms) value of phase current. The fundamental amplitude of flux density B_{m1} generated by magnetomotive force F_1 is:

$$B_{m1} = \frac{\mu_0}{\delta'} F_1 = \frac{\mu_0}{\delta'} \frac{\sqrt{2}m}{2} \frac{N_1 k_{w1}}{p} I_1 \quad (12)$$

where μ_0 is the vacuum permeability ($\mu_0 = 4\pi \times 10^{-7} \text{H/m}$). δ' is the air gap magnetic path length ($\delta' = \delta + 2h_m$). δ is the effective air gap length and h_m is the thickness of PM.

TABLE 2. Reactance and impedance of winding at different speeds.

Speed (r/min)	Reactance (Ω)	Impedance (Ω)	Reactance-to-impedance ratio ξ
100	0.080	2.002	4.07%
200	0.169	2.007	8.46%
300	0.259	2.017	12.88%
400	0.314	2.024	15.53%
500	0.362	2.032	17.81%

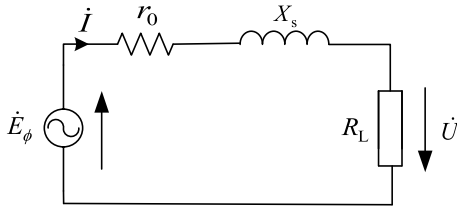


FIGURE 6. The single-phase equivalent circuit of PCB winding.

The flux linkage ψ_1 of armature reaction is:

$$\psi_1 = \frac{1}{\sqrt{2}} N_1 k_{w1} \frac{2}{\pi} B_{m1} \frac{\pi}{8p} (D_{mo}^2 - D_{mi}^2) \quad (13)$$

The inductance L_1 of armature reaction is:

$$L_1 = \frac{\psi_1}{I_1} = \frac{3\mu_0}{\pi \delta'} \left(\frac{N_1 k_{w1}}{2p} \right)^2 (D_{mo}^2 - D_{mi}^2) \quad (14)$$

At different speeds, the reactance generated by PCB winding will change accordingly with the frequency of magnetic field. In this section, the reactance, the impedance and the reactance-to-impedance ratio ξ of winding in the speed range from 100 r/min to 500 r/min are calculated and shown in Table 2. It can be concluded that the reactance-to-impedance ratio is lower at low speed.

D. OUTPUT POWER

When PCB generator is operating at load, the back-EMF of the generator will be induced in PCB winding and the output characteristics at load are given. The single-phase equivalent circuit of PCB winding is shown in Fig. 6.

Where E_ϕ is the rms value of back-EMF of PCB winding. r_0 is the internal resistance of PCB winding. X_s is the synchronous reactance of PCB winding. R_L is the value of load-resistance.

The equations of output current I_{out} , output voltage U_{out} and output power P_{out} in single-phase circuit of PCB winding are as follows:

$$I_{out} = \frac{E_\phi}{\sqrt{(r_0 + R_L)^2 + X_s^2}} \quad (15)$$

$$U_{out} = \frac{E_\phi \cdot R_L}{\sqrt{(r_0 + R_L)^2 + X_s^2}} \quad (16)$$

$$P_{out} = \frac{E_\phi^2 \cdot R_L}{(r_0 + R_L)^2 + X_s^2} \quad (17)$$

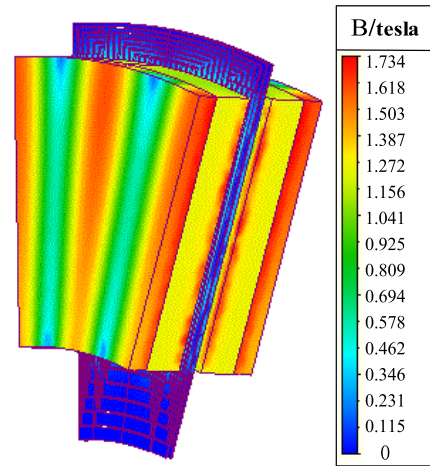


FIGURE 7. The magnetic flux density distribution of machine.

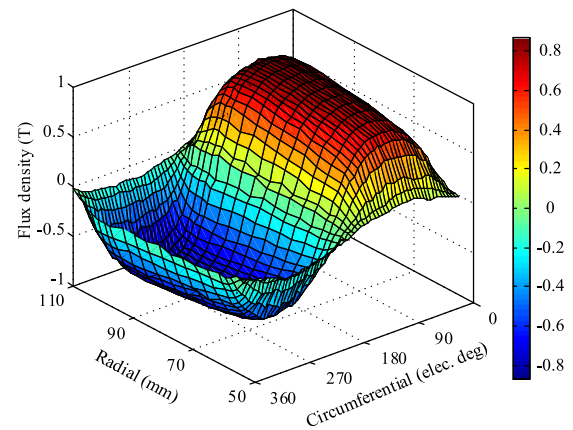


FIGURE 8. The 3-D flux density distribution diagram of air gap taken at different positions in the directions of circumferential and radial on the axial center surface of air gap under a pair of poles.

IV. COMPARISON ANALYSES

In this section, the FEA and analytical calculation are used to compare the electromagnetic performance of PCB generator between EW winding and UEW winding. The flux density distribution of PCB generator is analysed. The back-EMF and eddy-current loss of PCB generator at no-load are compared. The output characteristics of PCB generator, such as output current, output voltage and output power, are analysed.

A. FLUX DENSITY AT NO-LOAD CONDITION

When PCB generator is running at no-load, the flux density distribution cloud diagram of PCB generator is shown in Fig. 7. The 3-D flux density distribution diagram of air gap taken at different positions in the directions of circumferential and radial direction on the axial centre surface of air gap under a pair of poles as shown in Fig. 8.

On the basis of Fig. 8, the harmonic analysis of flux density is carried out by taking a circumferential distribution curve at average radius, as shown in Fig. 9. The fundamental wave amplitude of flux density in the air gap is 0.9 T. The total

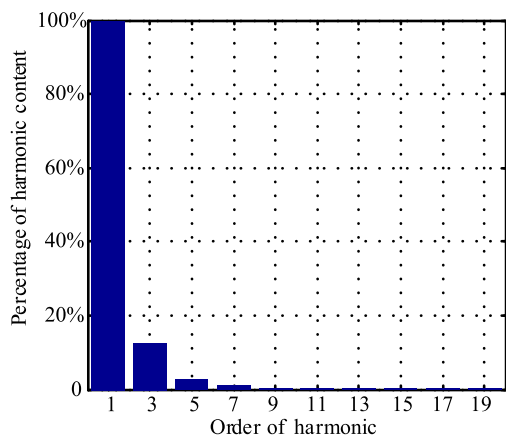


FIGURE 9. The harmonic analysis of flux density of circumferential distribution at average radius of air-gap.

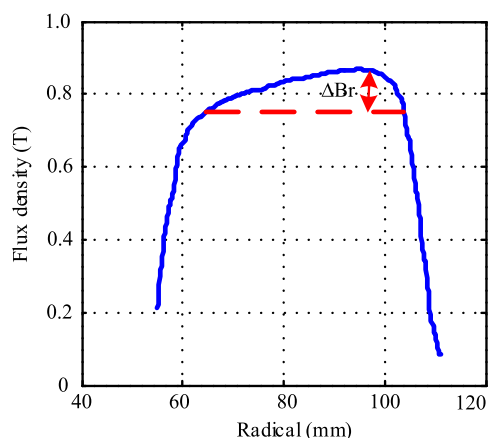


FIGURE 10. The flux density distribution in circumferential position of 90° electrical angle along the radial position at a pair of poles.

harmonic distortion (THD) rate is 13.6% and its 3rd harmonic distortion rate is 9.8%. The air gap flux density distribution in circumferential position of 90° electrical angle under a pair of poles is analysed along radial position, as shown in Fig. 10. The trend of flux density distribution gradually increases from the inner diameter to the outer diameter of PM and its difference value of flux density ΔBr is 0.12 T.

B. BACK EMF AND EDDY CURRENT LOSS AT NO-LOAD CONDITION

The curves of back EMF and eddy current loss of PCB winding with different speeds of the PCB generator at no-load can be obtained. The comparison curves of back-EMF for EW winding and UEW winding at different speeds under no-load condition are shown in Fig. 11. There values of EW winding and UEW winding by FEA are basically same with analytical calculation. Fig. 12 shows the comparison curves of eddy current loss for EW winding and UEW winding with different speeds at no-load state. The values obtained by analytical calculation are smaller than FEA and their average

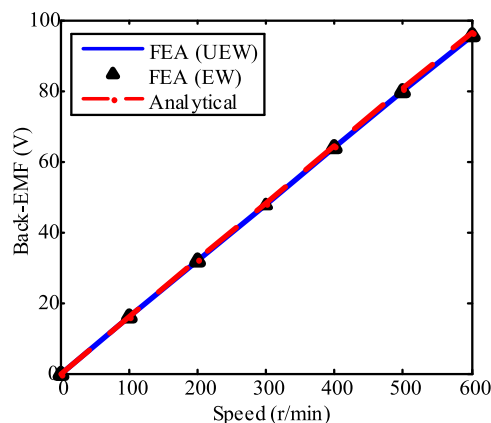


FIGURE 11. The comparison curves of back-EMF at different speeds in no-load condition.

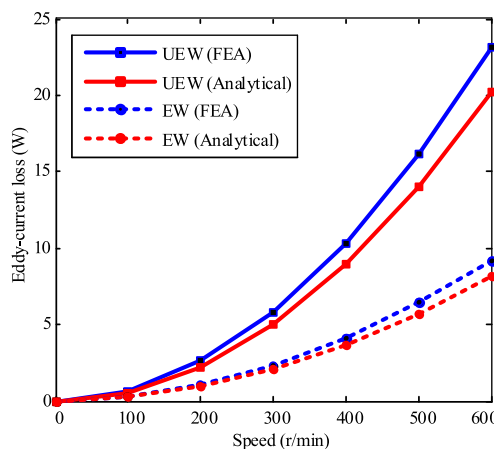


FIGURE 12. The comparison curves of eddy-current loss at different speeds in no-load condition.

value of deviation is about 13.4%. The value of eddy current loss produced by UEW winding is about 2.5 times that of EW winding at different speeds. When PCB generator is operating at rated speed of 300 r/min, the eddy current loss generated by FEA of UEW winding and EW winding is 6.0 W and 2.5 W respectively, which respectively account for 2.5% and 1.0% of rated output power. The increment of eddy current loss generated by UEW winding is only 1.5%, which has less effect on the output power of PCB generator.

C. OUTPUT CHARACTERISTICS AT LOAD CONDITION

For the convenience of comparison analysis between EW winding and UEW winding, this section compares output characteristics of the PCB generator under pure resistance load. Because of the smaller reactance X_s of PCB winding at low speed shown in Table 2, the magnitude of X_s^2 relative to $(R_L + r_0)^2$ can be ignored (R_L is larger than r_0 in this section) according to (15)-(17). Thus these equations (15)-(17) can be simplified into these equations (18-20), and the simplified analytical expressions of output current I'_{out} , output

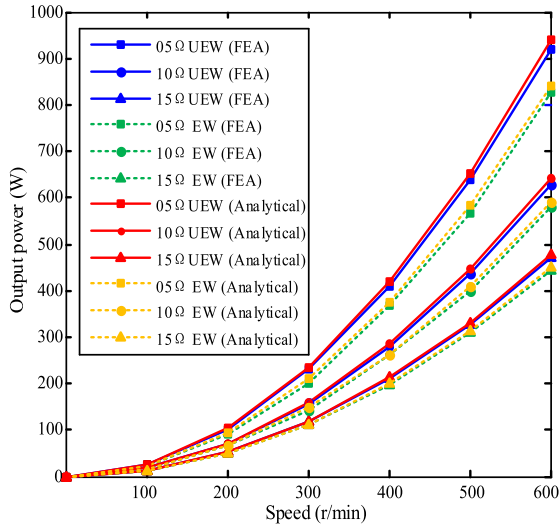


FIGURE 13. The comparison curves of output power changing with different speeds for EW winding and UEW winding of PCB generator at different loads.

voltage U'_{out} , and output power P'_{out} are as follows:

$$I'_{out} = \frac{1}{r_0 + R_L} E_\phi \quad (18)$$

$$U'_{out} = \frac{R_L}{r_0 + R_L} E_\phi \quad (19)$$

$$P'_{out} = \frac{R_L}{(r_0 + R_L)^2} E_\phi^2 \quad (20)$$

Fig. 13 shows the comparison curves of output power for EW winding and UEW winding with different speeds at load. It can be seen that the output power of the PCB generator with proposed UEW winding increases more obviously. When PCB generator is operating at rated speed with three load resistances of 15 Ω, 10 Ω, and 5 Ω, the output powers of proposed UEW winding by FEA are improved by 4.5%, 7.4%, and 10.7% respectively compared with conventional EW winding. Finally, the values of analytical calculation and FEA are compared. These comparison results are basically consistent, which verifies the effectiveness of the simplified analytical expressions.

On the basis of Fig. 13, the output characteristic curves of PCB generator with EW winding and UEW winding at rated speed are analysed separately. The comparison curves of output voltage with respect to output current for the two kinds of winding at rated speed of 300 r/min are shown in Fig. 14. It is shown that the results of analytical calculation are basically consistent with that of FEA. For conventional EW winding, when the limit of current density of active conductor is 12 A/mm² [10], the rms value of output current of EW winding is 4.1 A. Its output voltage obtained by FEA is 30.4 V and its voltage regulation rate is 57.8%. For proposed UEW winding, the current density at the inner end of active conductor is Maximum and its heating in this area is the most serious. Thus, it is more appropriate to compare and analyse with the conventional EW active conductor taking the current

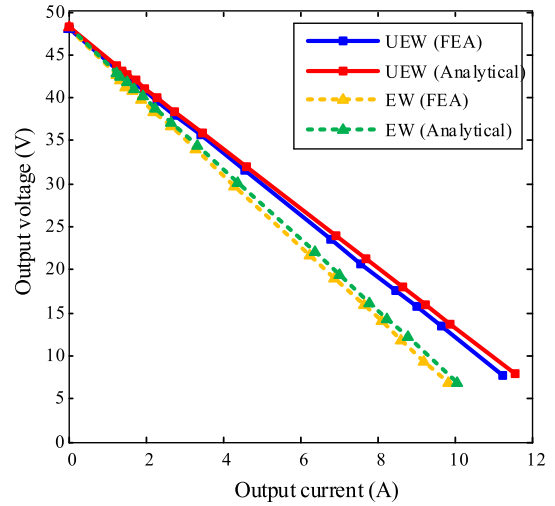


FIGURE 14. The comparison curves of output voltage with respect to the output current for EW winding and UEW winding of PCB generator at rated speed of 300 r/min.

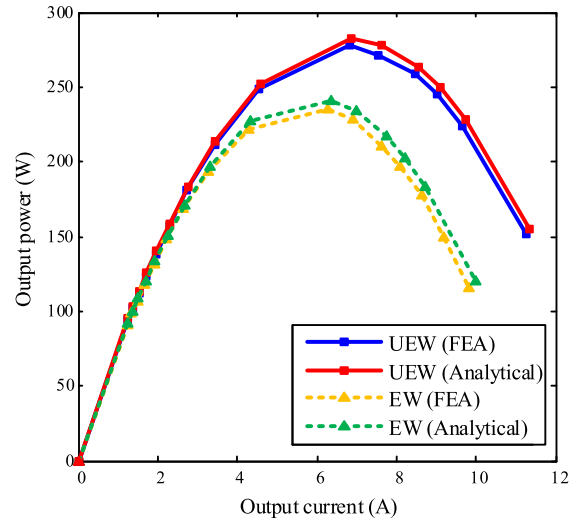


FIGURE 15. The comparison curves of output power changing with the output current for EW winding and UEW winding of PCB generator at rated speed of 300 r/min.

density at the inner end of the UEW active conductor as reference because the current density at the inner end of proposed UEW active conductor is same as that of conventional EW active conductor. When the current density of proposed UEW active conductor is 12 A/mm², its rms value of output current is also 4.1 A. Then its output voltage obtained by FEA is 33.3 V and its voltage regulation rate is 44.2%, which is reduces by 13.6% compared with that of the conventional EW PCB winding.

Fig. 15 shows the comparison curves of output power changing with the output current for EW winding and UEW winding of the PCB generator at rated speed of 300 r/min. These values of analytical calculation are also basically consistent with the values of FEA. It can be seen from Fig. 15 that there are peak values of output power corresponding to the

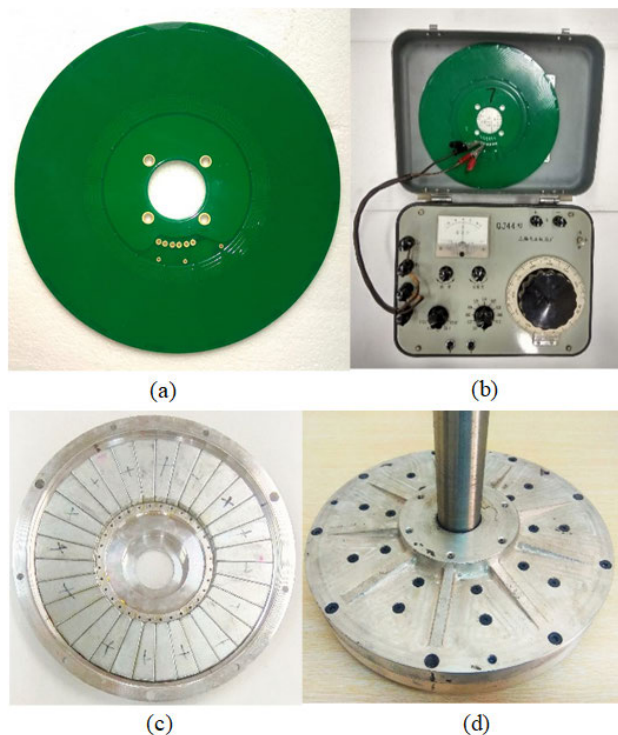


FIGURE 16. The designed PCB AFPM generator. (a) Actual PCB winding. (b) The resistance test device of DC double-arm Bridge. (c) Rotor disk with surface mounted PM segments. (d) The assembled machine.

two kinds of winding. The peak powers of conventional EW winding and proposed UEW winding obtained by FEA are 235 W and 278 W respectively, and its corresponding output currents are 6.3 A and 6.8 A respectively. However, it needs to consider the temperature limit of the PCB generator during normal operation. The output current of PCB generator cannot exceed 4.1 A (according to the experimental data in [10], the current density of active conductor is limited within 12 A/mm² to ensure normal operation of PCB generator. Thus its corresponding output current is within 4.1 A). Therefore, PCB generator with the two kinds of winding cannot run at the point of peak power at rated speed of 300 r/min. When the output current of the generator is 4.1 A by FEA, the output power of conventional EW winding is 216 W, and the output power of proposed UEW winding is 236 W, which is increased by 9.3%.

V. PROTOTYPE MACHINE TEST

In order to verify the validity of machine model and the accuracy of simulation results, the prototype of generator with proposed UEW PCB winding is made according to these design parameters of the machine. Fig. 16 shows the designed AFPM generator with PCB winding. The phase resistance of PCB winding measured by DC double-arm Bridge is 2.15 Ω, but its simulation value is 2.00 Ω, which is reduced by 7.0%. The error in the resistances between measured and simulated value, mainly derives from the influence of the copper sinking process of PCB. The prototype machine with proposed UEW PCB winding and its testing setup are shown in Fig. 17.

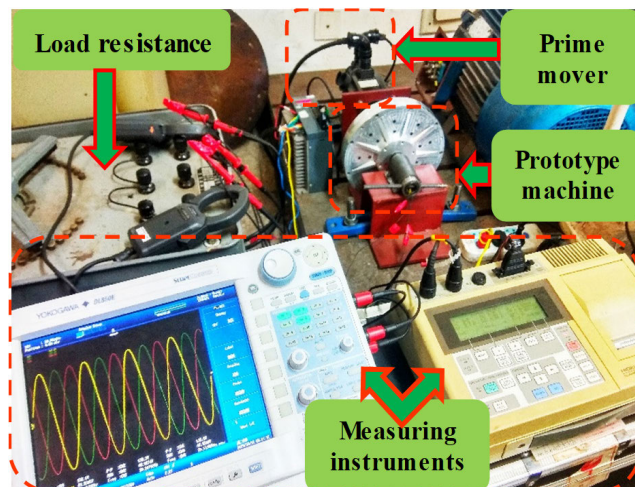


FIGURE 17. The testing setup of designed prototype machine.

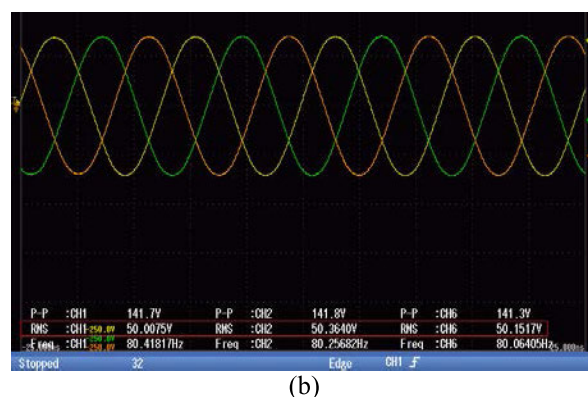
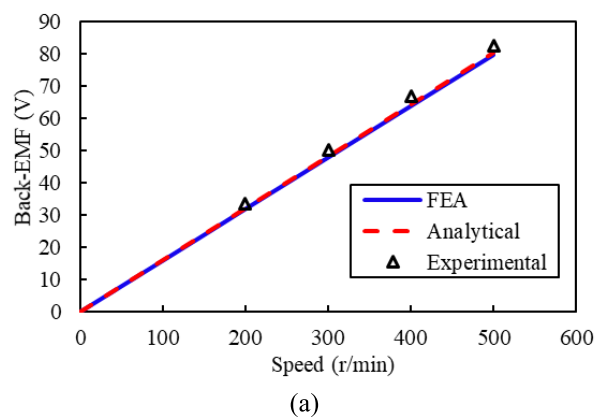


FIGURE 18. The back-EMF of prototype machine. (a) The comparison curves of back-EMF with respect to speed among FEA, analytical and experimental. (b) The experimental waveform of 3-phase back-EMF at rated speed of 300r/min.

The prototype machine with proposed UEW PCB winding is driven by prime machine and the load of prototype machine is pure resistive. The back-EMF is an important parameter for the generator. Through the experimental testing, the measured back-EMF is basically consistent with that of FEA and analytical calculation, shown in Fig. 18. The measured waveform of 3-phase back-EMF at rated speed

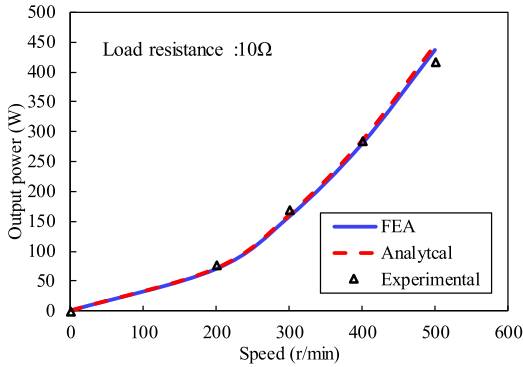


FIGURE 19. The comparison curves of output power with respect to speed among FEA, analytical and experimental at load resistance of 10.0 Ω.

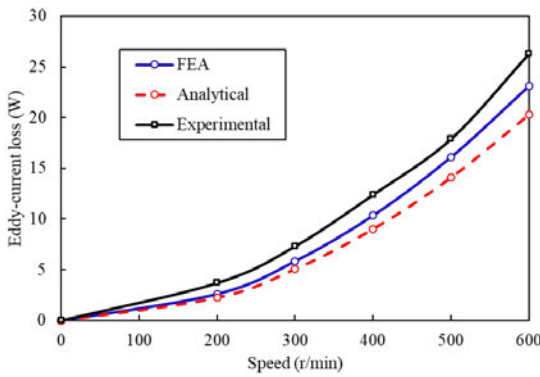


FIGURE 20. The comparison curves of Eddy-current losses with respect to speed among FEA, analytical and experimental.

of 300 r/min is nearly perfect sinusoidal, which means that the proposed generator has a good performance. Fig. 19 shows the output power curves with respect to the speed at the load resistance of 10.0 Ω. Since the winding reactance is very small at low speeds, it can be ignored relative to the total impedance. So the measured output power is almost proportional to the square of the speed. In order to measure the eddy current losses in PCB winding and efficiency of the prototype machine. The input power, output power and the basic copper loss are measured at different rotating speeds. The mechanical losses are considered as 1.5% of the input power at low speeds, estimated as [22]. Ignoring the losses in PMs and rotor disks, the eddy current losses in PCB winding can be indirectly measured, shown in Fig. 20. Because the losses in PMs and rotor disks are neglected, the eddy current loss in PCB winding measured by experimental is 23.5% larger than that of FEA. Though the difference percentage of eddy current loss between experiment and FEA is larger, the eddy current loss of PCB winding itself is smaller, which leads to that the difference of eddy current loss between experiment and FEA is smaller. At the same time, the result also shows that the neglected losses in PMs and rotor disks are smaller.

The efficiency of the prototype machine at different speeds is shown in Fig. 21. The efficiency of prototype machine

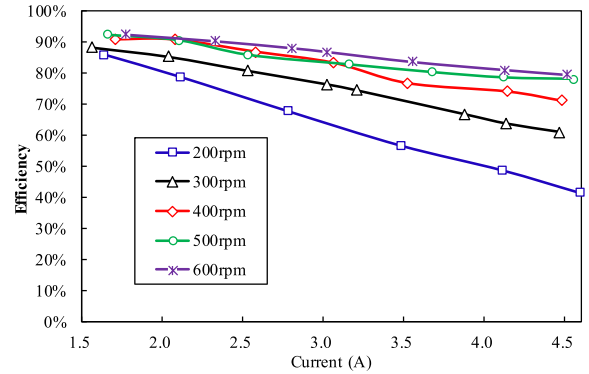


FIGURE 21. The efficiency of the prototype machine at different rotating speeds.

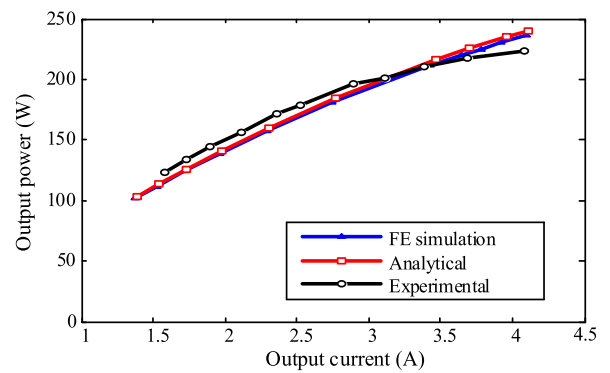


FIGURE 22. The comparison curves of output power with respect to output current among FEA, analytical and experimental at rated speed of 300 r/min.

decreases gradually with the increase of the load current. This is mainly because the copper loss (the mainly source of losses of PCB machine) increases with square multiple of load current. However, the output power of prototype machine increases approximately with one time of load current within certain current range. So it results in the reduction of the efficiency of machine with the increase of load current. What's more, the efficiency of prototype machine generally improves with the increase of the rotating speed for the same load current. The reason is that the copper loss is almost constant for the same load current. But the back-EMF increases with the increase of the rotating speed, which results in the increase of the output power of the prototype machine. Although the eddy current loss increases with the increase of the rotating speed, it accounts for a smaller proportion of the total losses and can be ignored. So the efficiency generally increases with the increase of the rotating speed for the same load current.

In order to verify the output power of the prototype machine at rated speed of 300r/min, the output power curves with respect to the load current is shown in Fig. 22. By comparison, these output powers calculated by FEA and analytical calculation are basically consistent with the output power measured by experiment, which verifies the validity of the FEA and analytical formulas. When the load current

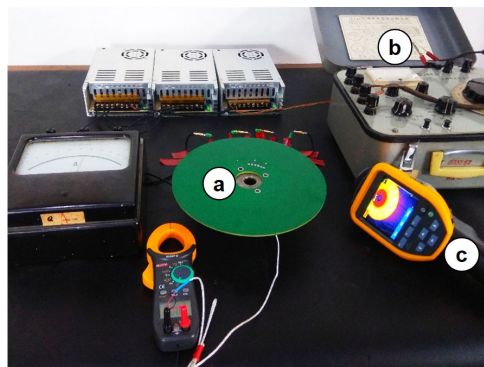


FIGURE 23. The temperature testing setup of PCB winding. (a)PCB winding. (b)DC double-arm Bridge. (c) Infrared thermal camera.

of prototype machine is 4.1 A, the output power is 223 W, which is basically consistent with the expected output power. However, the efficiency of the prototype machine is only 63.8%. The main source of losses in the machine is from copper loss of PCB winding. In order to verify the idea that the copper loss of PCB winding has a great impact on the efficiency of the generator, the experiment of reducing the copper loss by decreasing the load current has been done. The result shows that when the load currents are respectively 0.75 times and 0.5 times of the rated current, the efficiency of the prototype machine are 76.5% and 85.4%, respectively. It indicates that the copper loss of PCB winding impacts on the efficiency of the generator greatly. In the next design, the number of parallel layers of PCB winding may be increased to reduce the resistance and copper loss of PCB winding, which can improve the efficiency of the generator.

For small wind-power AFPM generators, the losses in PMs and rotor disks is very small due to the lower harmonic component of the air gap flux density and the lower rotating speed of the machine, which can be ignored. Therefore, the main source of losses in the machine is PCB winding losses (including basic copper losses and eddy current losses of PCB winding). As the main heat source of the motor, it will cause the temperature rising of the PCB winding which may impair the performance of the machine. If the temperature rising of PCB winding is too high, the machine may be burned down. So it is necessary to perform some thermal analyses towards PCB winding and the prototype machine. The temperature rising testing setup of PCB winding is shown in Fig. 23. Through the experiment of the natural cooling at ambient temperature of 27.0°C, the stabilized temperature of PCB winding operating at the current density of 12 A/mm² is about 110.2°C (temperature rising about 83.2°C), shown in Fig. 24. Because the high temperature gradient (TG) of FR4 (the substrate material of PCB) is above 170.0°C, the PCB winding can steadily operate at the current density of 12 A/mm².

As the PCB winding is inside the prototype machine, it is difficult to obtain temperature data of PCB winding by infrared thermal camera. However, the temperature of PCB

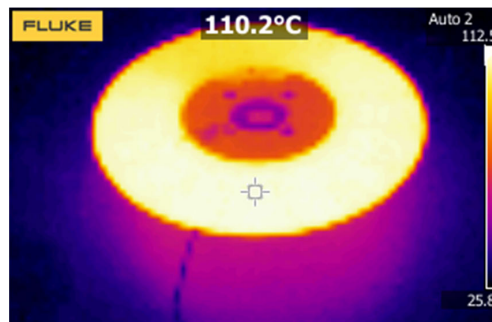


FIGURE 24. The thermal mapping of PCB winding operating at the current density of 12A/mm².

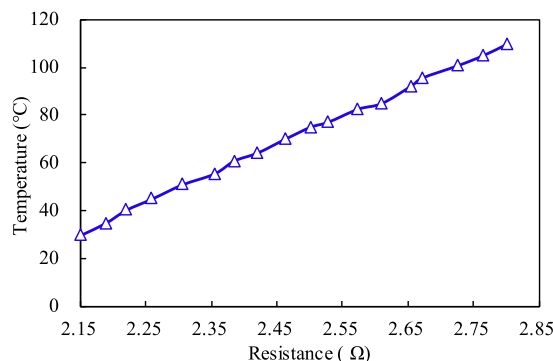


FIGURE 25. The temperature curve of the PCB winding with respect to the phase-resistance of the PCB winding.

winding can be measured indirectly by measuring the phase resistance of PCB winding because the resistance of PCB winding varies with the temperature. Therefore, these phase-resistance data corresponding to these temperature data of PCB winding have been measured at the natural cooling. These temperature data are obtained by infrared thermal camera. Finally, the temperature curve of PCB winding with respect to the phase-resistance of PCB winding is shown in Fig. 25. The phase-resistance of PCB winding is almost proportional to the temperature.

Then, the prototype machine operates continuously under rated conditions of the current density of 12 A/mm² for 2 hours. The phase-resistance of PCB winding is measured quickly by the DC double-arm bridge at the end of the machine operation. The phase-resistance of PCB winding is 2.675 Ω. According to the curve in Fig.25, the corresponding stable temperature is about 95.0°C (temperature rising about 68.0°C), which is high and shows the poor thermal performance. The main reason is that the PCB windings are enclosed in the machine housing. Although there is thermal convection between the PCB windings and the rotor which takes away a large amount of the heat of PCB winding, the heat is blocked by the sealed machine housing. It causes the heat to not be released in time, which leads to the high temperature in PCB winding. This is the defect of the mechanical structure design of the prototype machine. A few slots should be made around the housing to promote the heat

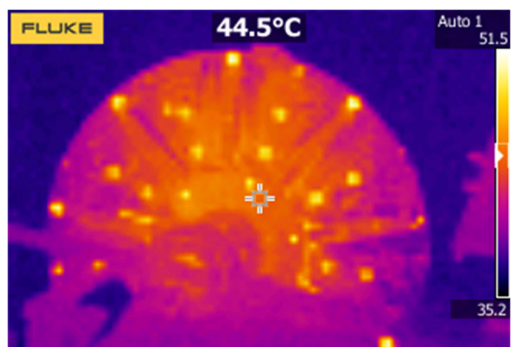


FIGURE 26. The thermal mapping of the prototype machine operating under rated condition of the current density of $12\text{A}/\text{mm}^2$.

dissipation of the PCB winding. The thermal mapping of the prototype machine is shown in Fig. 26. The ambient temperature is 27.0°C . The housing temperature of the prototype machine is lower, about 44.5°C . Because the housing of the prototype machine is rotating, which can take away a large amount of heat from the machine surface.

For the AFPM machine equipped with conventional wire winding, the current density of the stator winding is generally $3\text{ A}/\text{mm}^2$ – $6\text{ A}/\text{mm}^2$ under the air-cooling condition [3], [23]–[25]. The main reason is that a large number of heat generated by the stator windings is concentrated inside the slots of the machine, so it is difficult to be released in time. This results in a higher temperature rising of the stator windings. Thus, the stable temperature rising of the conventional wire winding in the AFPM machine [23]–[25] is generally 70°C – 80°C under the air-cooling condition. However, the stable temperature rising of PCB winding in the prototype machine is about 30°C under the air-cooling condition while the current density of PCB winding is $6\text{ A}/\text{mm}^2$. The result shows that the AFPM machine with PCB windings has an excellent thermal performance in comparison to that of conventional wire windings in the same current density. As this paper focuses on the analysis and design of the electromagnetic performance of the machine, the detailed theoretical and experimental research on the thermal performance of the machine is being in process, but beyond the scope of this paper.

VI. CONCLUSION

In this article, a new type of UEW PCB winding and its design ideas are proposed for AFPMG. Through FEA and analytical calculation, these characteristics of the PCB generator with traditional EW winding and proposed UEW winding are analysed and compared in detail, and verified by prototype machine. These conclusions are obtained as follows: 1) For the design of proposed UEW PCB winding, it's necessary to consider these characteristics of electromagnetic and manufacture technology of the PCB. Through these analyses for PCB winding and experiments on prototype machine, the feasibility of design ideas of PCB winding is verified. 2) Comparing with conventional EW PCB winding, the

proposed UEW PCB winding has the advantages of smaller resistance, larger equivalent heat dissipation area and average current carrying capacity. 3) For this small wind turbine with PCB winding operating at low speed, proposed UEW PCB winding has less effect on eddy current loss than conventional EW PCB winding. By comparisons, the voltage regulation rate of UEW winding is reduced by 13.6% and its output power is increased by 9.3%. Through the thermal experiment of the prototype machine, the result shows that the AFPMG with PCB windings has an excellent thermal performance in comparison to that of conventional wire windings.

REFERENCES

- [1] A. Daghighi, H. Javadi, and H. Torkaman, "Design optimization of direct-coupled ironless axial flux permanent magnet synchronous wind generator with low cost and high annual energy yield," *IEEE Trans. Magn.*, vol. 52, no. 9, Sep. 2016, Art. no. 7403611.
- [2] S. Javadi and M. Mirsalim, "Design and analysis of 42-V coreless axial-flux permanent-magnet generators for automotive applications," *IEEE Trans. Magn.*, vol. 46, no. 4, pp. 1015–1023, Apr. 2010.
- [3] F. G. Capponi, G. De Donato, and F. Caricchi, "Recent advances in axial-flux permanent-magnet machine technology," *IEEE Trans. Ind. Appl.*, vol. 48, no. 6, pp. 2190–2205, Nov./Dec. 2012.
- [4] W. Deng, S. Zuo, F. Lin, and S. Wu, "Influence of pole and slot combinations on vibration and noise in external rotor axial flux in-wheel motors," *IET Electr. Power Appl.*, vol. 11, no. 4, pp. 586–594, Apr. 2017.
- [5] Y. S. Ayat and M. R. A. Pahlavani, "3D computation of no-load magnetic flux density in slotless axial-flux permanent-magnet synchronous machines using conformal mapping," *IET Electr. Power Appl.*, vol. 11, no. 8, pp. 1391–1396, Sep. 2017.
- [6] S. J. Arand and M. Ardebili, "Multi-objective design and prototyping of a low cogging torque axial-flux PM generator with segmented stator for small-scale direct-drive wind turbines," *IET Electr. Power Appl.*, vol. 10, no. 9, pp. 889–899, Nov. 2016.
- [7] M. Shokri, N. Rostami, V. Behjat, J. Pyrhönen, and M. Rostami, "Comparison of performance characteristics of axial-flux permanent-magnet synchronous machine with different magnet shapes," *IEEE Trans. Magn.*, vol. 51, no. 12, Dec. 2015, Art. no. 8115206.
- [8] P. Jin, Y. Yuan, Q. Xu, S. Fang, H. Lin, and S. L. Ho, "Analysis of axial-flux Halbach permanent-magnet machine," *IEEE Trans. Magn.*, vol. 51, no. 11, Nov. 2015, Art. no. 8207404.
- [9] J. F. Wu, "Design of a miniature axial flux flywheel motor with PCB winding for nanosatellites," in *Proc. Int. Conf. Opt. Micro. (ICOM)*, 2012, pp. 544–548.
- [10] X. Y. Wang and C. Zhou, "Thermal analysis and cooling approach design of axial flux permanent magnet synchronous machines with PCB winding," *Proc. Csee*, vol. 36, no. 11, pp. 3062–3069, Jun. 2016.
- [11] X. Y. Wang, C. P. Li, and F. Lou, "Geometry optimize of printed circuit board stator winding in coreless axial field permanent magnet motor," in *Proc. IEEE Vehicle Power Pro. Conf. (VPPC)*, Oct. 2016, pp. 1–6.
- [12] H. Wang, J.-F. Wu, Y. Li, and Y.-H. Wu, "PCB stator winding in axial flux permanent magnet motor for reaction flywheel system," *Opt. Precis. Eng.*, vol. 23, no. 4, pp. 1004–1010, Apr. 2015.
- [13] S. Moury and M. T. Iqbal, "A permanent magnet generator with PCB stator for low speed marine current applications," in *Proc. 1st Int. Conf. Develop. Renew. Energy Technol. (ICDRET)*, Dec. 2009, pp. 1–4.
- [14] T. Reed and E. Bakhom, "Axial flux permanent magnet alternator using printed circuit board stators," in *Proc. IEEE SoutheastCon*, Apr. 2008, pp. 454–459.
- [15] M. C. Tsai and L. Y. Hsu, "Design of a miniature axial-flux spindle motor with rhomboidal PCB winding," *IEEE Trans. Magn.*, vol. 42, no. 10, pp. 3488–3490, Oct. 2006.
- [16] R. Y. Tang, *Theory and Design of Modern Permanent Magnet Machines*. Beijing, China: China Machine Press, 2016, pp. 309–329.
- [17] Z. Q. Qi, "Experience and understanding of high-speed PCB design," *Electron. Des. Eng.*, vol. 19, no. 16, pp. 141–143, Aug. 2011.
- [18] Q. Dong, J. Ni, and Y. Liu, "The wiring design of PCB and anti-jamming technology," *Ship Sci. Technol.*, vol. 28, no. 2, pp. 57–59, Apr. 2006.

- [19] A. A. Arkadan, T. M. Hijazi, and B. Masri, "Design evaluation of conventional and toothless stator wind power axial-flux PM generator," *IEEE Trans. Magn.*, vol. 53, no. 6, Jun. 2017, Art. no. 8104404.
- [20] R.-J. Wang and M. J. Kamper, "Calculation of eddy current loss in axial field permanent-magnet machine with coreless stator," *IEEE Trans. Energy Convers.*, vol. 19, no. 3, pp. 532–538, Sep. 2004.
- [21] R. J. Wang, M. J. Kamper, K. Van der Westhuizen, and J. F. Gieras, "Optimal design of a coreless stator axial flux permanent-magnet generator," *IEEE Trans. Magn.*, vol. 41, no. 1, pp. 55–64, Jan. 2005.
- [22] R. Wrobel, G. Vainel, C. Copeland, T. Duda, D. Staton, and P. H. Mellor, "Investigation of mechanical loss components and heat transfer in an axial-flux PM machine," *IEEE Trans. Ind. Appl.*, vol. 51, no. 4, pp. 3000–3011, Jul. 2015.
- [23] G. Vainel, D. A. Staton, F. G. Capponi, G. De Donato, and F. Caricchi, "Thermal modelling of a fractional-slot concentrated-winding Kaman type axial-flux permanent-magnet machine," in *Proc. IEEE Energy Convers. Congr. Expo. (ECCE)*, Sep. 2013, pp. 1505–1511.
- [24] F. Marignetti, V. D. Colli, and Y. Coia, "Design of axial flux PM synchronous machines through 3-D coupled electromagnetic thermal and fluid-dynamical finite-element analysis," *IEEE Trans. Ind. Electron.*, vol. 55, no. 10, pp. 3591–3601, Oct. 2008.
- [25] J. R. Bumby and R. Martin, "Axial-flux permanent-magnet air-cored generator for small-scale wind turbines," *IET Electr. Power Appl.*, vol. 152, no. 5, pp. 1065–1075, Sep. 2005.



WEI PANG was born in Hubei, China, in 1993. He received the B.E. degree in electrical engineering from the Shenyang University of Technology, Shenyang, China, in 2017. Since 2017, he is currently pursuing the M.E. degree in electrical engineering with the School of Electrical and Information Engineering, Tianjin University, Tianjin, China. His current research interests include the design of PCB stator winding and the research of axial flux permanent magnet machine with PCB stators.



PENG GAO was born in Hebei, China, in 1985. He received the B.E. degree in electrical engineering from the Shenyang University of Chemical Technology, Shenyang, China, in 2009, and the M.E. and Ph.D. degrees in electrical engineering from Tianjin University, Tianjin, China, in 2011 and 2015, respectively. Since 2015, he has been a Lecturer with the School of Electrical and Information Engineering, Tianjin University. His current research interests include the design of electrical machines, drive motor system for electric vehicles, and motors for high speed applications.



XIAOYUAN WANG was born in Hebei, China, in 1962. He received the B.E. and M.E. degrees in electrical engineering from Tianjin University, Tianjin, China, in 1982 and 1985, respectively, and the Ph.D. degree in electrical engineering from the Shenyang University of Technology, Shenyang, China, in 2006. Since 2007, he has been a Professor with the School of Electrical and Information Engineering, Tianjin University. His current research interests include the design of electrical machines, drive motor system for electric vehicles, motors for high speed applications, and the research of axial flux permanent magnet machines.



XIAOXIAO ZHAO was born in Hebei, China, in 1995. She received the B.E. degree in electrical engineering from the Shenyang University of Technology, Shenyang, China, in 2017. Since 2017, she is currently pursuing the M.E. and Ph.D. degrees in electrical engineering with the School of Electrical and Information Engineering, Tianjin University, Tianjin, China. Her current research interests include the design of axial flux permanent magnet machines and the drive motor system design for electric vehicles.

...